Impact of size distributions of major chemical components in fine particles on light extinction in urban Guangzhou

CrossMark

Yunjie Xia [a,b,*], Jun Tao [c], Leiming Zhang [d], Renjian Zhang [b,**], Shuanglin Li [e], Yunfei Wu [b], Junji Cao [f], Xiaojia Wang [b], Qingxia Ma [b], Zhe Xiong [b]

[a] College of Atmospheric Sciences, Chengdu University of Information Technology, Plateau Atmosphere and Environment Key Laboratory of Sichuan Province, Chengdu, China
[b] CAS Key Laboratory of Regional Climate-Environment for Temperate East Asia, Institute of Atmospheric Physics, Chinese Academy of Sciences, Beijing, China
[c] South China Institute of Environmental Sciences, Ministry of Environmental Protection, Guangzhou, China
[d] Air Quality Research Division, Science Technology Branch, Environment and Climate Change Canada, Toronto, Canada
[e] Nansen-Zhu International Research Centre, Institute of Atmospheric Physics, Chinese Academy of Sciences, Beijing, China
[f] Key Laboratory of Aerosol, SKLLQG, Institute of Earth Environment, Chinese Academy of Sciences, Xi'an, China

HIGHLIGHTS

- Aerosol chemical components in PM_1 and $PM_{1-2.5}$ were compared in two seasons.
- The size distributions of chemical components varied with pollution levels.
- Contributions of chemical components in PM_1 and $PM_{1-2.5}$ to light extinction were quantified.

GRAPHICAL ABSTRACT
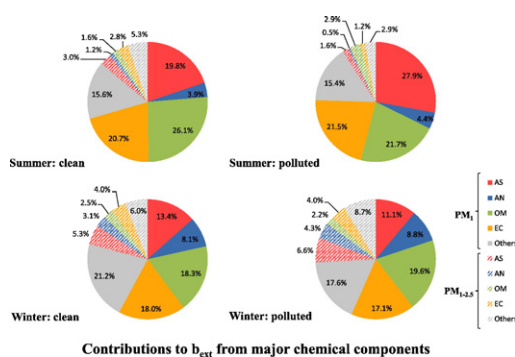
Contributions to b_{ext} from major chemical components

ARTICLE INFO

ABSTRACT

To evaluate the impact of fine particulate matter ($PM_{2.5}$) size distribution on aerosol chemical and optical properties, dominant chemical components including water-soluble inorganic ions (WSII), organic carbon (OC) and elemental carbon (EC) in PM_1 and $PM_{2.5}$, aerosol scattering coefficient (b_{sp}), and aerosol absorption coefficient (b_{ap}) were collected synchronously at an urban site in Guangzhou, south China during a typical summer month in 2009 and a winter month in 2010. PM_1 (sizes smaller than 1 μm) constituted 77% and 63% of $PM_{2.5}$ in summer and winter, respectively. From the reconstructed mass concentrations, the sum of SO_4^{2-}, NO_3^- and NH_4^+ (SNA) distributed more in PM_1 than in $PM_{1-2.5}$ ($PM_{2.5}$ minus PM_1) in summer and the opposite was found in winter, while carbonaceous aerosols distributed more in PM_1 in both summer and winter. With the aggravation of $PM_{2.5}$ pollution, the mass fraction of $PM_1/PM_{2.5}$ increased for $(NH_4)_2SO_4$ (AS), NH_4NO_3 (AN) and EC but decreased for organic matter (OM) in summer, and the opposite was found in winter. B_{sp} of PM_1 and $PM_{1-2.5}$ was estimated from the mass extinction efficiencies (MSEs) of the dominant chemical components, which showed good correlations ($R^2 = 0.99$) with measured ones and those estimated

* Corresponding author at: CAS Key Laboratory of Regional Climate-Environment for Temperate East Asia, Institute of Atmospheric Physics, Chinese Academy of Sciences, Beijing, China.
** Corresponding author.
E-mail addresses: xiayunjie@mail.iap.ac.cn (Y. Xia), zrj@mail.iap.ac.cn (R. Zhang).

using the IMPROVE formula. The fractional contributions of dominant chemical components to extinction coefficient (b_{ext}) were consistent with their respective mass size distributions, indicating the importance of chemically-resolved aerosol size distributions on aerosol optical properties and haze formation.

1. Introduction

High levels of particulate matter, especially $PM_{2.5}$ (aerodynamic diameter < 2.5 μm) have detrimental impacts on air quality and visibility, and thus human health, besides their roles on climate impact and ecosystem health (Samet et al., 2000; Malm et al., 2003; Ramanathan and Feng, 2009). The frequent hazy days occurred in recent years across China have spurred numerous investigations (Cheung et al., 2005; Zhang et al., 2013; Huang et al., 2014; Che et al., 2015a). Haze intensity can be characterized by the sum of aerosol light scattering and absorption (Watson, 2002), both strongly dependent on aerosol chemical components and associated size-distributions (Cozic et al., 2008; Lin et al., 2013). Multivariable regression models and empirical formulas are commonly used for investigating the relationships between aerosol optical properties and $PM_{2.5}$ components. Secondary inorganic aerosols (SIA), OM and EC in $PM_{2.5}$ have been identified as the dominant contributors to light extinction (Hand and Malm, 2007). However, these chemical species are mainly distributed in PM_1 (Aiken et al., 2009; Sun et al., 2011), and the MSEs of submicron particles with diameters close to wavelength of visual light are much larger than those of the coarse particles (Bergin et al., 2001; Cheng et al., 2008; Che et al., 2015b). It is important to quantify the contributions of PM_1 on the total aerosol optical properties and its role on haze formation.

The Pearl River Delta (PRD) region is one of the three megacity clusters in China, where have been frequently suffering haze weather in recent years (Wang et al., 2003; Andreae et al., 2008; Deng et al., 2008). Field experiments have been conducted in PRD to identify the causes of haze (Hu et al., 2008; Zhang et al., 2010; Yue et al., 2010; Tao et al., 2017). In some studies, the Mie Model and the IMPROVE formula were used to identify major chemical components contributing to light extinction (Liu et al., 2009b; Tao et al., 2014). Most of these studies focused on the physical and chemical characteristics of aerosols and their relationships with optical properties. Studies explored the size fractions of PM have also been conducted in PRD (Cheng et al., 2008; Jung et al., 2009); however, few studies have explored the relative contributions of PM_1 and $PM_{1-2.5}$ on haze formation.

To fill this knowledge gap, chemically-resolved PM_1 and $PM_{2.5}$, b_{sp}, and b_{ap} were collected at an urban site in Guangzhou during a summer month in 2009 and a winter month in 2010. The size distributions of major chemical components were first briefly characterized in Section 3.1, followed by discussions on their differences under different pollution levels (Section 3.2). Chemical factors contributing to b_{ext} were then quantified in Section 3.3.

2. Methodology

2.1. Site description

Measurements were collected at the monitoring station of the South China Institute of Environmental Science (SCIES) (23.12° N, 113.35° E) located in an urban area of Guangzhou. All instruments used in this study were installed on the roof of a building 50 m above the ground (Tao et al., 2014). The land is generally flat and there is no obvious industrial pollution source around the station. The data observed at this site largely represented air pollution levels in Guangzhou.

2.2. Sampling and chemical analysis

Daily (24 h from 10:00 am to 9:30 am the next day, local time) PM_1 and $PM_{2.5}$ samples were synchronously collected using particulate samplers (BGI Incorporated, Model PQ200) in a summer (July 1st to July 31st, 2009) and a winter (January 1st to January 31st, 2010) months. Samples were collected on 47 mm quartz filter (Whatman OM-A) with a flow rate of 16.7 L min^{-1}, baked at 800 °C for at least 3 h and equilibrated in desiccators for 24 h in advance. The exposed filter was stored in a freezer at minus 20 °C to prevent particle volatilization.

A punch of 0.5 cm^2 from each quartz filter was analyzed for eight carbon fractions following the IMPROVE TOR protocol by Desert Research Institute (DIR) model 2001 carbon analyzer (Atmoslytic Inc. Calabasas, CA) (Chow et al., 2004, 2007; Cao et al., 2007). Eight inorganic ions (SO_4^{2-}, NO_3^-, Cl^-, Na^+, NH_4^+, K^+, Mg^{2+} and Ca^{2+}) in aqueous extracts of the filter were determined by an ion chromatography (Dionex Corp, Sunnyvale, CA, Model Dionex 600).

2.3. Measurements and corrections of aerosol optical properties

b_{sp} was measured at three wavelengths (450, 550 and 700 nm) with an integrating nephelometer (TSI Performance Measurement Tools, Model 3563) equipped with a conventional total suspended particulate (TSP) cyclone. The flow rate was set at 20 L min^{-1} for drawing air through a temperature controlled inlet, which controlled the relative humidity (RH) of inflow air to be <70% to minimize the influence of water vapor. Nephelometer calibration was carried out by carbon dioxide (CO_2) as a high span gas and by filtered air as a low span gas. The output data were set to be 1 min average, and the baseline data were measured hourly. The raw data of b_{sp} have been corrected for truncation and non-Lambertian illumination errors according to Anderson and Ogren (1998).

b_{ap} was measured using a 7-channel aethalometer (Magee Scientific Company, US, Model AE31) which is used for real time measurement of black carbon (BC). The aethalometer was equipped with a conventional total suspended particulate (TSP) cyclone and the flow rate was set at 5 L min^{-1}. The aethalometer was calibrated to zero by replacing the filter in the canister inlet with a clean filter every week. In this study, a direct method proposed by Weingartner et al. (2003) was used to obtain b_{ap} with correction parameters based on Wu et al. (2012, 2013).

2.4. Data analysis methods

2.4.1. Reconstruction of PM mass

To evaluate whether the determined chemical components represent the measured PM_1 and $PM_{1-2.5}$, the measured PM_1 and $PM_{2.5}$ masses were reconstructed based on AS (1.375 SO_4^{2-}), AN (1.29 NO_3^-), OM, and EC. The converting factor between OM and OC was chosen as 1.6 (Feng et al., 2009; Zhang et al., 2013). Unidentified chemical species, termed as the "Other" here, can be estimated by subtracting the sum of the determined chemical species mentioned above from the measured PM_1 or $PM_{2.5}$ mass concentrations. $PM_{1-2.5}$ was obtained by subtracting PM_1 from $PM_{2.5}$.

2.4.2. Estimation of b_{sp} of PM_1 and $PM_{1-2.5}$

The reconstructed chemical components in Section 2.4.1, which were also the major contributors to b_{sp}, were used to estimate b_{sp} of PM_1 and $PM_{1-2.5}$. An external mixing of individual species was assumed in the analysis. Due to the lack of information on the size distributions of the chemical components, the densities and MSE curves of the major

chemical species were applied to firstly determine MSEs of PM_1 and $PM_{1-2.5}$.

$$\rho = \sum_i M_i / \sum_i \frac{M_i}{\rho_i} \tag{1}$$

$$D = D_a \cdot \frac{1}{\sqrt{\rho}} \tag{2}$$

In Eq. (1), ρ_i is the assumed density of a chemical species (Watson, 2002; Cheng et al., 2008; Lin et al., 2013), M_i refers to the mass concentration of the reconstructed chemical component, ρ stands for the average density of the total particle. In Eq. (2), D is the particle volumetric equivalent diameter and is calculated based on D_a (the median cut-off aerodynamic diameter). D_a can be estimated by the median value of the upper and lower boundaries of PM_1 or $PM_{1-2.5}$. MSE of each chemical species can then be obtained from the curves of MSE size distribution (Tao et al., 2015). Total scattering coefficient of PM_1 or $PM_{1-2.5}$ can be estimated statistically using individual chemical species concentrations and corresponding MSEs.

2.4.3. Reconstruction of b_{ext}

b_{ext} includes the contributions from b_{sp} and b_{ap}:

$$b_{ext} = b_{sp} + b_{ap} \tag{3}$$

$$b_{ap} = 8.28 \times [EC] \tag{4}$$

where b_{sp} was obtained from the results estimated in Section 2.4.2, and b_{ap} of 550 nm was estimated using an experienced converting factor of 8.28 $m^2\,g^{-1}$ (Yan et al., 2008; Wu et al., 2009). For comparison, the revised IMPROVE formula was used to estimate b_{sp} of $PM_{2.5}$:

$$\begin{aligned} b_{sp}(revised) = & 2.2 \times f_s(RH) \times [Small\ (NH_4)_2SO_4] \\ & + 4.8 \times f_L(RH) \times [Large\ (NH_4)_2SO_4] \\ & + 2.4 \times f_s(RH) \times [Small\ NH_4NO_3] \\ & + 5.1 \times f_L(RH) \times [Large\ NH_4NO_3] \\ & + 2.8 \times [Small\ OM] + 6.1 \times [Large\ OM] \\ & + 1.7 \times f_{ss} \times [SS] + 1.0 \times [FS] + 0.6 \times [CM] \end{aligned} \tag{5}$$

$$[Large\ X] = [Total\ X]^2/20, \quad [Total\ X] < 20, \tag{6}$$

$$[Large\ X] = [Total\ X], \quad [Total\ X] \geq 20, \tag{7}$$

$$[Small\ X] = [Total\ X] - [Large\ X] \tag{8}$$

where AS $[(NH_4)_2SO_4] = 1.375\ [SO_4^{2-}]$; AN $[NH_4NO_3] = 1.29\ [NO_3^-]$; $[OM] = 1.6\ [OC]$; Sea Salt $[SS] = 1.8\ [Cl^-]$; Fine Soil $[FS] = 2.2$ $[Al] + 2.49\ [Si] + 1.94\ [Ti] + 1.63\ [Ca] + 2.42\ [Fe]$; Coarse Mass $[CM] = [PM_{10}] - [PM_{2.5}]$; and X represent sulfate, nitrate, and OM mass concentrations, respectively. B_{sp} and mass concentrations are given in units of Mm^{-1} and $\mu g\,m^{-3}$, respectively. RH growth curves of sulfate ($f_s(RH)$), nitrate ($f_L(RH)$), and SS ($f_{ss}[RH]$) are referred to Pitchford et al. (2007). Due to the lack of soil elements of PM, the FS mass was assumed to be 20 times of Ca^{2+} based on previous soil source profiles (Amato and Hopke, 2012). Daily PM_{10} concentrations were obtained from a national environmental monitoring station (Shangxueyuan nearby SCIES). In this study, RH data were obtained from an inner RH detector inside a nephelometer rather than an ambient RH detector (i.e., precision reached 0.1%).

2.4.4. Air mass back trajectory analysis

To identify the causes of size- and pollution-level dependent chemical components, 48-h back trajectories were calculated using the Trajstat software (Wang et al., 2009) based on Geographic Information System. Global Data Assimilation System (GDAS) meteorological dataset (ftp://arlftp.arlhq.noaa.gov/pub/archives/gdas/) was used as input. The trajectories were initialized at 6:00 UTC every 24 h and the arrival level was set at 100 m a.g.l. 31 trajectories in any selected month (season) were classified into two pollution levels – clean and polluted periods (more discussion below).

3. Results and discussion

3.1. Size distribution of chemical components

The average mass concentrations of PM_1 and $PM_{1-2.5}$ ($PM_{2.5}$ minus PM_1) were $29.9 \pm 13.3\ \mu g\,m^{-3}$ and $8.7 \pm 3.1\ \mu g\,m^{-3}$, respectively, in summer and $63.4 \pm 30.2\ \mu g\,m^{-3}$ and $39.9 \pm 21.8\ \mu g\,m^{-3}$, respectively, in winter (Fig. 1). Both PM_1 and $PM_{1-2.5}$ were more than doubled in winter than in summer. PM_1 constituted 77% and 63% of $PM_{2.5}$ in summer and winter, respectively. The $PM_1/PM_{2.5}$ fraction of the major chemical components generally followed that of PM_1. For example, OC in PM_1 accounted for 82% and 74% of OC in $PM_{2.5}$ in summer and winter, respectively; while for EC, 86% and 78%, respectively. Thus, OC and EC in $PM_{2.5}$ were mainly distributed in PM_1. SO_4^{2-}, NO_3^- and NH_4^+ (SIA) were the dominant water-soluble inorganic ions, and together accounted for 76% and 83% of WSII in $PM_{2.5}$ during summer and winter, respectively. The lower levels of SIA in summer were likely due to clean monsoon and precipitation scavenging of aerosols, as well as by higher temperature which was conducive for the evaporation of ammonium nitrate, further decreasing NO_3^- and NH_4^+ than SO_4^{2-}. NH_4^+ in PM_1 accounted for 79% and 63% of NH_4^+ in $PM_{2.5}$ in summer and winter, respectively, similar to those of NO_3^- (65% and 56%) and carbonaceous fractions (OC and EC) mentioned above. However, SO_4^{2-} in PM_1 accounted for 83% of SO_4^{2-} in $PM_{2.5}$ in summer, which was much higher than 57% in winter. The lower percentage of SO_4^{2-} in PM_1 in winter was likely due to a large fraction of $CaSO_4$, as evidenced by the higher Ca^{2+} concentration (Tao et al., 2014). Ca^{2+} is indeed preferentially combined with SO_4^{2-} according to the aerosol thermodynamic equilibrium model (Lin et al., 2013; Fountoukis and Nenes, 2007).

PM_1 and $PM_{1-2.5}$ mass concentrations were reconstructed based on AS, AN, OM and EC mass concentrations (Fig. 2). Good correlations ($R^2 > 0.95$) were found between the reconstructed and measured PM mass, indicating that the above chemical components closely represented the measured PM. By comparison, the results of the reconstruction in summer were better than those in winter. It reveals that fine particle mass variability is controlled by submicron particles in summer (Fig. 3).

AS and AN were considered to be the dominant components of secondary aerosols, which play an important role in the haze formation (Huang et al., 2014). In this study, AS and AN together accounted for 41% and 35% of PM_1 and $PM_{1-2.5}$, respectively, in summer, and 37% and 47% in winter. Thus, they contributed slightly more to PM_1 than $PM_{1-2.5}$ in summer and the opposite was found in winter. Carbonaceous aerosols (OM + EC) were also among the major components of fine particles, contributing about 36% and 23% to PM_1 and $PM_{1-2.5}$, respectively, in
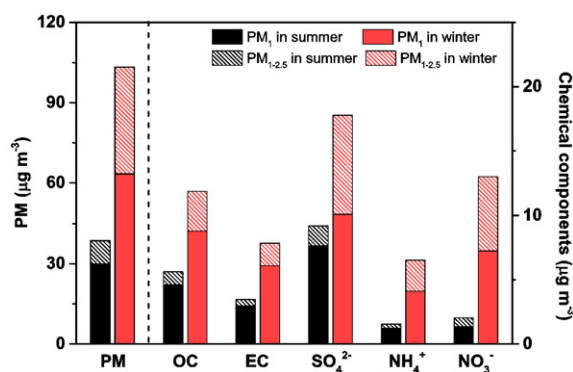
Fig. 1. Concentrations of PM mass and major chemical components (WSII, OC, and EC) in PM_1 and $PM_{1-2.5}$.
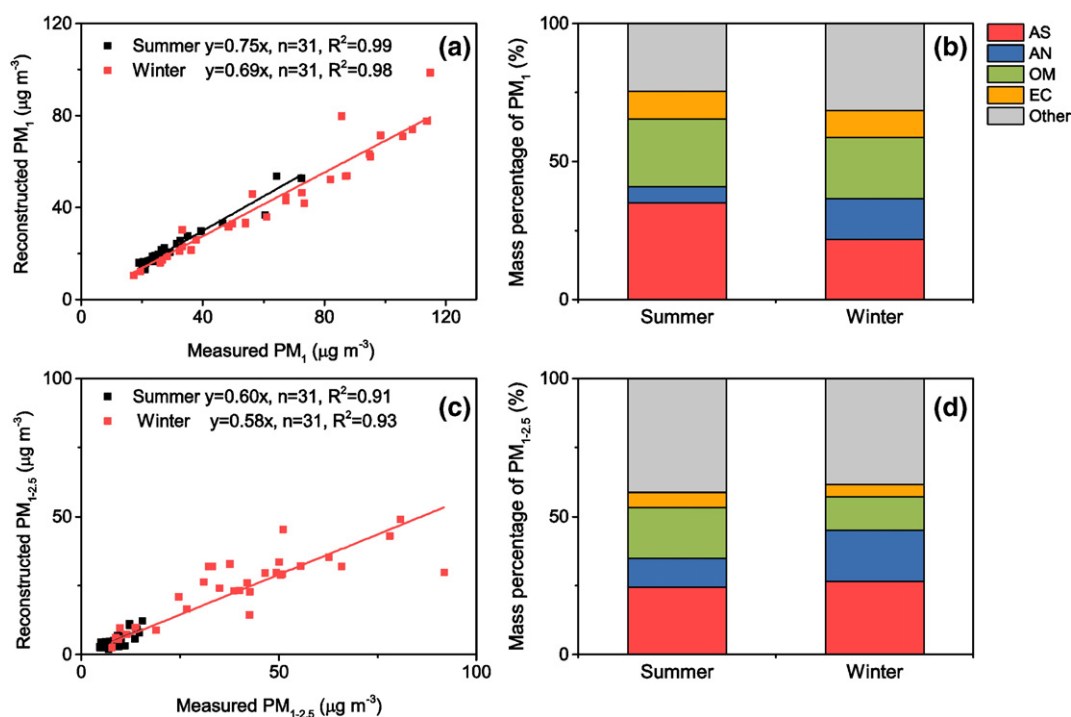
Fig. 2. Relationships between the measured and reconstructed mass concentrations of PM_1 (a) and $PM_{1-2.5}$ (c) and the corresponding mass fractions of major chemical components (b and d).

summer, and 31% and 18% in winter. Generally, the contributions of carbonaceous aerosols were slightly lower than that of AS and AN.

3.2. Size distribution characterization on polluted days

To explore the variation of size distribution of dominant chemical components with pollution levels, the measurement data were categorized into two different pollution levels: the clean day with $PM_{2.5}$ below 75 μg m^{-3} and the polluted day with $PM_{2.5}$ above this value. 29 clean and 2 polluted days were observed in the summer month, and 9 clean days and 22 polluted days were observed in the winter month. In the summer month wind directions were predominantly from the south (Fig. 5a). The large proportion of clean days was because of the transport of clean air from the South China Sea. Polluted days occurred when the air masses were from inland and with poor diffusion conditions leading accumulation of air pollutants (Fig. 5b). During the summer month, the two polluted episodes were mainly related to the two Tropical Storms. There reported that an area of low pressure on 9 July 2009 in
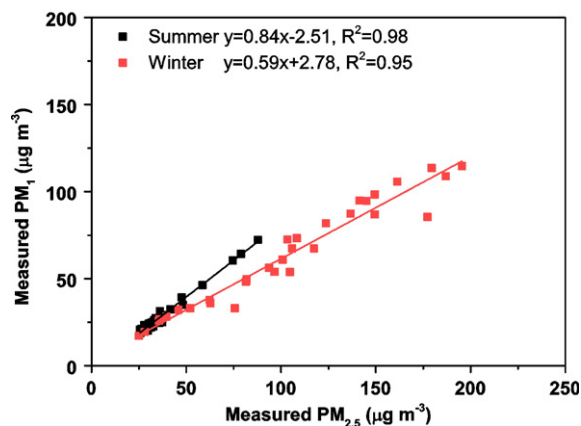
Fig. 3. Relationships between the measured PM_1 and $PM_{2.5}$ mass concentrations.

Guangzhou led to the high pollutant levels on the next day. The Tropical Storm Soudelor brushed the northern part of South China Sea on July 11 and then reduced pollution rapidly. Similarly, Typhoon Molave formed on July 16 could be used to explain another polluted day occurred on July 17.

As shown in Fig. 4a, the proportion of PM_1 to $PM_{2.5}$ rose from 77% on clean days to 82% on polluted days in the summer month. While the proportions of AS, AN and EC increased accordingly, OM showed an opposite trend. Fast conversion of SO_2 to SO_4^{2-} due to high temperature combined with regional transport from atmospheric recirculation caused the accumulation and aging of sulfate aerosols in summer (Cusack et al., 2013). In contrast, AN should be mainly locally formed since high temperature is conducive for the evaporation of nitrate and thus regional transport played a minor role in the accumulation of nitrate at the measurement site. Some studies indicated that carbonaceous aerosols were mainly distributed in the submicron particles (Chen et al., 1997). In Guangzhou, vehicle emissions were the dominant sources of carbonaceous aerosols in summer (Tao et al., 2014). The proportions of EC in PM_1 to EC in $PM_{2.5}$ increased from 85% on clean days to 93% on polluted days. Note that OM can be easily oxidized from smaller sizes to larger ones under higher O_3 condition (Liu et al., 2009a).

The proportion of PM_1 to $PM_{2.5}$ decreased from 66% on clean days to 61% on polluted days in the winter month (Fig. 4b). It should be noted that the proportion of AS and AN in $PM_{1-2.5}$ increased significantly on polluted days, likely related to the hygroscopic growth of AS and AN under high RH conditions during the winter (Tao et al., 2014; Che et al., 2014). Besides, previous studies confirmed that relatively large and aged particles can be transported to Guangzhou from the sea by the eastern or southeastern winds (Cheng et al., 2006). On clean days (Fig. 5c), air masses mainly came from north of Guangzhou where few emission located compared with those from south directions. When air mass origins changed from northeasterly inland to southeastern coast, air pollution aggravated. The air masses along the coast were stable and maintained at low to middle altitudes, which likely carried high levels of pollutants from the coastal industrial belts. The differences in the size distributions of carbonaceous aerosols between clean and polluted days were not so obvious in winter as in summer. Especially, the
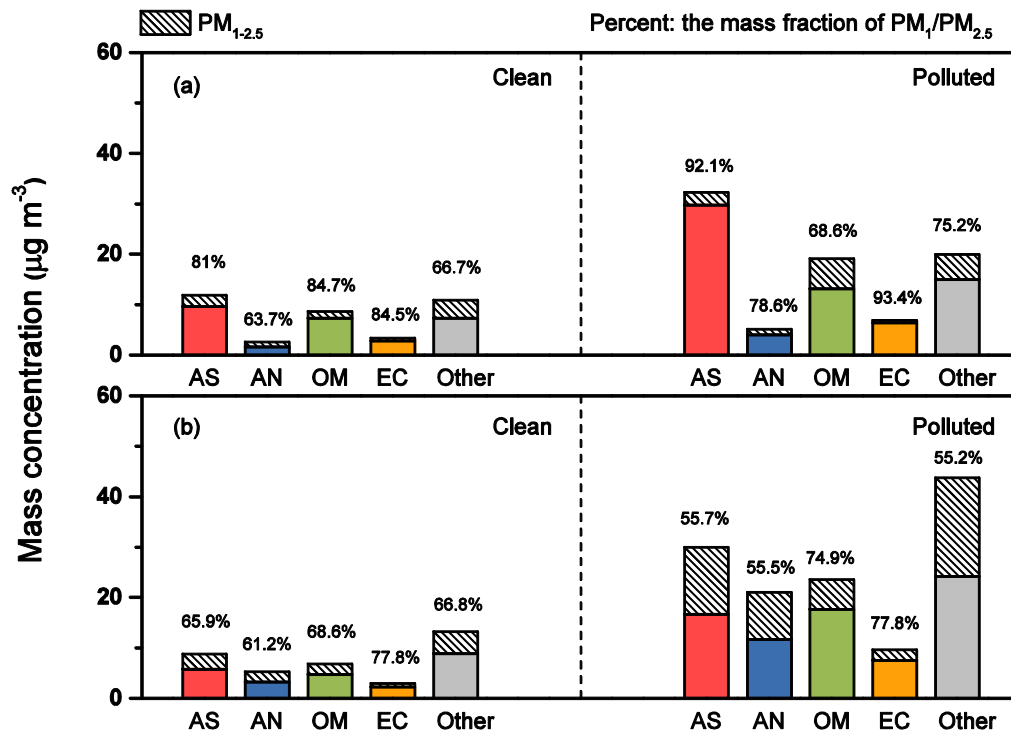
Fig. 4. Mass concentrations and proportions of chemical components in PM_1 and $PM_{1-2.5}$ on clean and polluted days (a: summer; b: winter).

proportion of OM in PM_1 to that in $PM_{2.5}$ increased rather than decreased on polluted days than clean days in winter. Coal combustion and vehicle exhaust were the dominant sources of carbonaceous aerosols in winter (Tao et al., 2014), and coal combustion produced carbonaceous aerosols were largely in small size particles.

In summary, the size distributions of major chemical components showed obvious differences between summer and winter. AS, AN, and

EC but not OM showed the same trend with PM_1. The proportions of AS, AN, and EC in PM_1 to those in $PM_{2.5}$ increased on summer polluted days compared to clean days while those of OM decreased. An opposite trend was found in winter for AS, AN, and OM. The different seasonal-dependent size distributions of dominant chemical components likely have important implications on haze formation and on aerosol optical properties, as further discussed below.
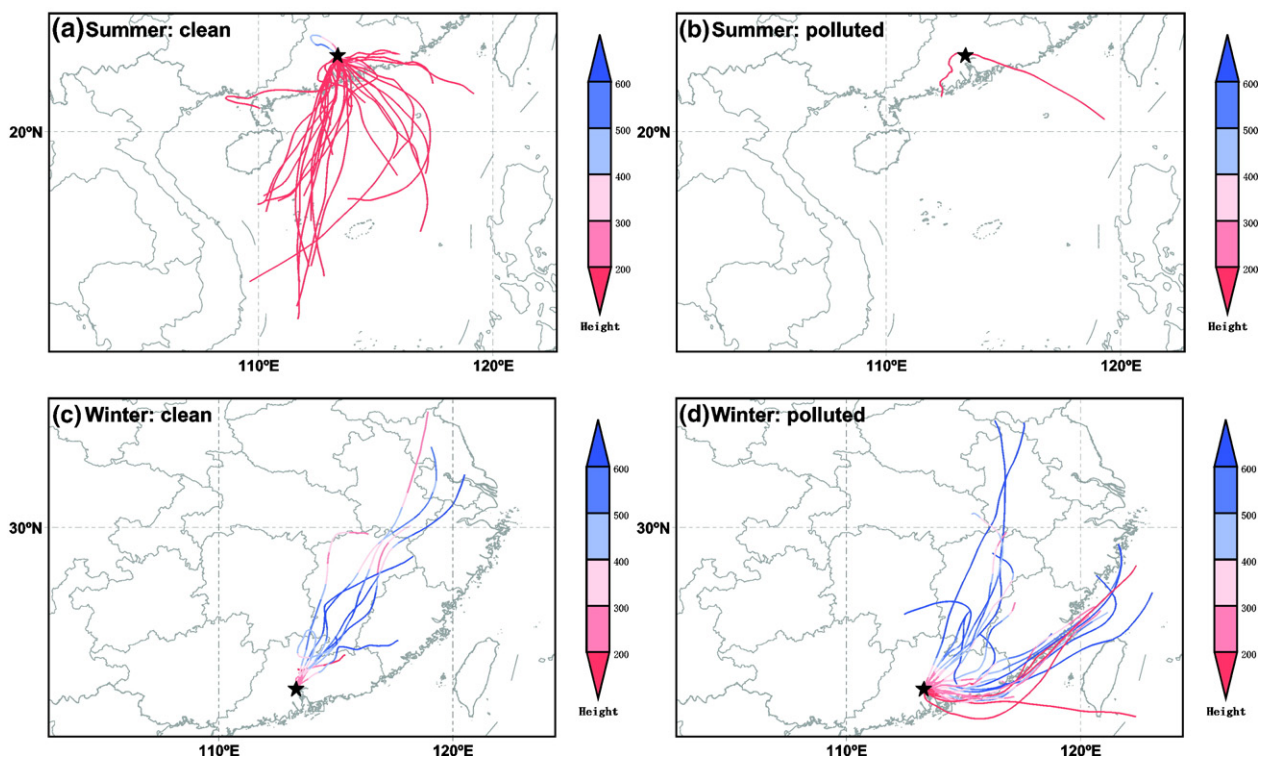
Fig. 5. The 48 h air mass backward trajectories starting at 100 m on clean and polluted days in summer and winter (colors in the legend represent the height of air masses).
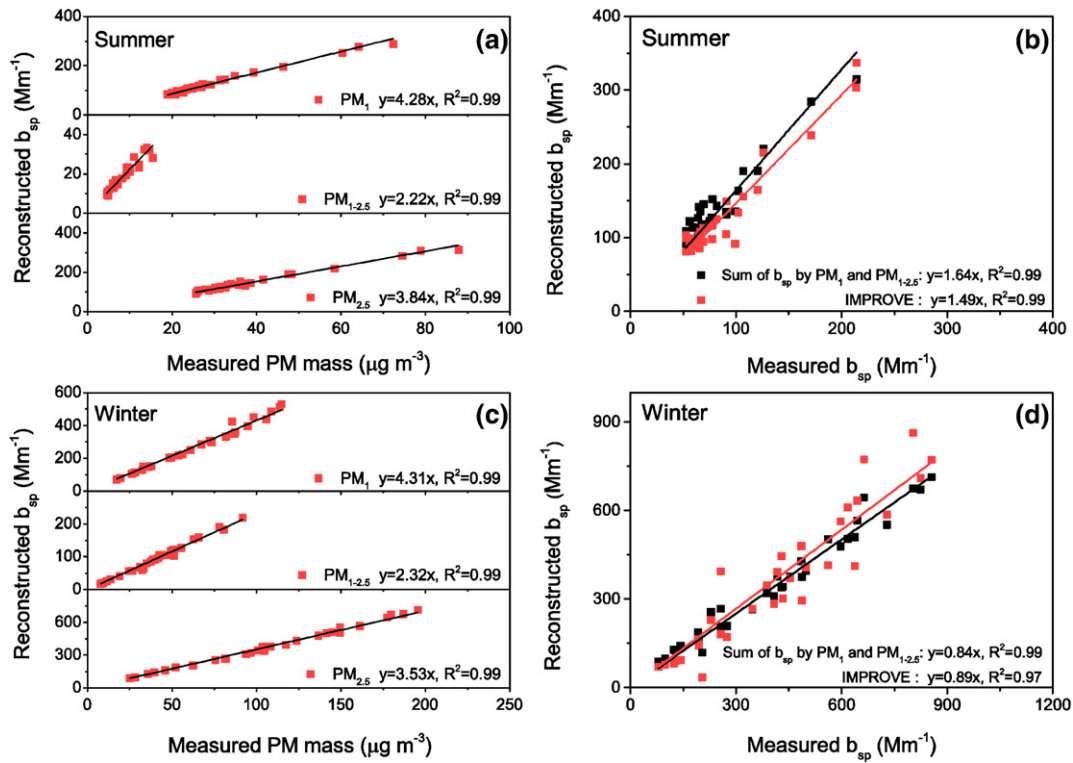
Fig. 6. Linear correlation between the measured PM mass and reconstructed b_{sp} (a, c), and the reconstructed b_{sp} of $PM_{2.5}$ by two methods versus measured b_{sp} (b, d).

3.3. Fractional contribution to extinction coefficients

To determine the impact of the size distributions of the major chemical components of $PM_{2.5}$ on light extinction, b_{sp} of PM_1 and $PM_{1-2.5}$ were reconstructed from MSEs of the dominant chemical species (described in Section 2.4.2 above). Strong correlations ($R^2 = 0.99$) were found between the reconstructed b_{sp} and the measured PM mass with slopes of close to 1.0 (Fig. 6a, c). The regression slopes can be treated as MSEs, which reflect the scattering ability of a unit mass of PM_1 or $PM_{1-2.5}$. Besides, the sum of b_{sp} by PM_1 and $PM_{1-2.5}$ was used to estimate the b_{sp} by $PM_{2.5}$. MSEs of PM_1, $PM_{1-2.5}$ and $PM_{2.5}$ in summer (4.3, 2.2 and 3.8 $m^2\,g^{-1}$, respectively) were close to those in winter (4.3, 2.3 and 3.5 $m^2\,g^{-1}$, respectively). MSEs of PM_1 were much higher than those of $PM_{1-2.5}$, consistent with Mie theory. MSEs of $PM_{2.5}$ in this study were comparable with that in Chengdu (3.5–4.4 $m^2\,g^{-1}$) and in Beijing (3.6–4.9 $m^2\,g^{-1}$) (Tao et al., 2014, 2015). The reconstructed b_{sp} of $PM_{2.5}$ were compared with the measured b_{sp} and the results obtained using the revised IMPROVE formula (Fig. 6b and d). In fact, the measured b_{sp} of $PM_{2.5}$ was not the real $PM_{2.5}$ MSE because of the TSP cyclone. However, the contribution of CM to b_{sp} was negligible, and the measured b_{sp} can be used to calculate $PM_{2.5}$ MSEs as a rough approximation (Tao et al., 2014). It can be seen that the estimated b_{sp} using the method described above was overestimated in summer and underestimated in winter compared to the measured b_{sp}, and the deviation was much higher in summer than winter. It can be inferred that b_{sp} measured by nephelometer in summer was likely underestimated.

This conclusion is supported by the distribution of deliquescence relative humidity (DRH) and equilibrium constant of K_p (Stelson and Seinfeld, 1982). According to the thermodynamic equilibrium theory, airborne particles were assumed to exist as aqueous solution when ambient RH > DRH and as solids when ambient RH < DRH. The condition (DRH > RH) is in favor of AN existing in the solid phase.

$$\ln(DRH) = 723.7/T + 1.7037 \tag{9}$$

$$\ln(K_p) = 84.6 - 24220/T - 6.1 * \ln(T/298) \tag{10}$$

Equilibrium constant K_p can also characterize the dissociation of ammonium nitrate in solid phase. Inside the nephelometer, RH was lower than DRH of AN. However, K_p was higher in summer but lower in winter (Fig. 7). This explains the significant volatility losses of AN in summer but not in winter. Thus, the measured b_{sp} by nephelometer should be underestimated to some extent in summer.
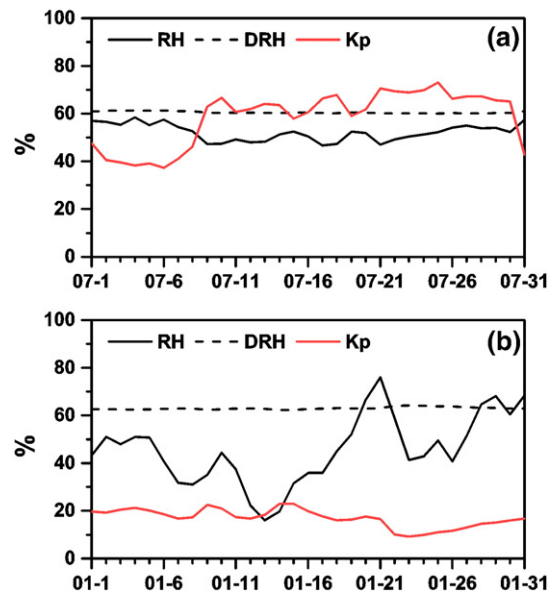
Fig. 7. Temporal variations of daily RH, DRH, and K_p within the nephelometer in summer (a) and winter (b).

Table 1
The contributions from dominant chemical components in PM_1 and $PM_{1-2.5}$ to the estimated b_{ext} in the different seasons and pollution levels.

	Clean (summer)		Polluted (summer)		Clean (winter)		Polluted (winter)	
	PM_1	$PM_{1-2.5}$	PM_1	$PM_{1-2.5}$	PM_1	$PM_{1-2.5}$	PM_1	$PM_{1-2.5}$
AS	19.8%	3.0%	27.9%	1.6%	13.4%	5.3%	11.1%	6.6%
AN	3.9%	1.2%	4.4%	0.5%	8.1%	3.1%	8.8%	4.3%
OM	26.1%	1.6%	21.7%	2.9%	18.3%	2.5%	19.6%	2.2%
EC	20.7%	2.8%	21.5%	1.2%	18.0%	4.0%	17.1%	4.0%
Other	15.6%	5.3%	15.4%	2.9%	21.2%	6.0%	17.6%	8.7%
Sum	86.1%	13.9%	90.9%	9.1%	79.0%	20.9%	74.2%	25.8%

The fractional contributions of each major chemical component to b_{ext} were calculated separately for the two pollution levels (Table 1). On average, PM_1 and $PM_{1-2.5}$ accounted for 86% and 14%, respectively, of b_{ext} in summer, and 76% and 24% in winter on clean days. With the pollution aggravating on polluted days, the contribution of PM_1 to b_{ext} increased to 91% in summer but decreased to 74% in winter. These fractional contributions to b_{ext} were consistent with the related PM mass concentrations. On polluted days in summer, the contributions of AS, AN, and EC in PM_1 to b_{ext} significantly increased while that of OM decreased, and the opposite trend was found in winter.

4. Conclusions

Major chemical components in PM_1 and $PM_{2.5}$ were analyzed in a summer and a winter months and under clean and polluted conditions in urban Guangzhou, south China. $PM_{1-2.5}$ components were extracted as the difference of those in PM_1 and $PM_{2.5}$. PM_1 and its major components dominated over $PM_{1-2.5}$ in both seasons. The reconstructed mass concentrations of PM_1 and $PM_{1-2.5}$ based on AS, AN, OM and EC suggested that the sum of AS and AN accounted for 41% and 35% of PM_1 and $PM_{1-2.5}$, respectively, in summer, and 37% and 47% in winter, while carbonaceous aerosols contributed 36% and 23% to PM_1 and $PM_{1-2.5}$, respectively, in summer, and 31% and 18% in winter.

Good relations ($R^2 = 0.99$) were found between the measured b_{sp} and the estimated b_{sp} or the reconstructed results from IMPROVE formula. However, b_{sp} measured by nephelometer in summer was underestimated due to the large volatility losses of AN. The percentage contribution of PM_1 to the total b_{ext} increased from 86% on clean days to 91% on polluted days in summer but declined from 79% to 74% in winter. On polluted days in summer, the percentage contributions of AS, AN, and EC in PM_1 to the total b_{ext} significantly increased while that of OM decreased, and the opposite was found for AS, AN, and OM in winter. These results suggest that chemically-resolved aerosol size distributions are important for complete understanding of aerosol optical properties and their impact on haze formation.

Acknowledgments

References

Aiken, A., Salcedo, D., Cubison, M.J., Huffman, J., DeCarlo, P., Ulbrich, I.M., 2009. Mexico City aerosol analysis during MILAGRO using high resolution aerosol mass spectrometry at the urban supersite (T0)—part 1: fine particle composition and organic source apportionment. Atmos. Chem. Phys. 9, 6633–6653.

Amato, F., Hopke, P.K., 2012. Source apportionment of the ambient $PM_{2.5}$ across St. Louis using constrained positive matrix factorization. Atmos. Environ. 46, 329–337.

Anderson, T.L., Ogren, J.A., 1998. Determining aerosol radiative properties using the TSI 3563 integrating nephelometer. Aerosol Sci. Technol. 29, 57–69.

Andreae, M.O., Schmid, O., Yang, H., Chand, D., Yu, J.Z., Zeng, L.M., 2008. Optical properties and chemical composition of the atmospheric aerosol in urban Guangzhou, China. Atmos. Environ. 42, 6335–6350.

Bergin, M.H., Cass, G.R., Xu, J., Fang, C., Zeng, L.M., Yu, T., 2001. Aerosol radiative, physical, and chemical properties in Beijing during June 1999. J. Geophys. Res. 106, 17969–17980.

Cao, J.J., Lee, S.C., Chow, J.C., Watson, J.G., Ho, K.F., Zhang, R.J., 2007. Spatial and seasonal distributions of carbonaceous aerosols over China. J. Geophys. Res. 112, D22S11.

Che, H., Xia, X., Zhu, J., Li, Z., Dubovik, O., Holben, B., 2014. Column aerosol optical properties and aerosol radiative forcing during a serious haze-fog month over north china plain in 2013 based on ground-based sunphotometer measurements. Atmos. Chem. Phys. 14, 2125–2138.

Che, H., Zhang, X., Xia, X., Goloub, P., Holben, B., Zhao, H., 2015a. Ground-based aerosol climatology of China: aerosol optical depths from the China Aerosol Remote Sensing Network (CARSNET) 2002–2013. Atmos. Chem. Phys. 15, 7619–7652.

Che, H., Xia, X., Zhu, J., Wang, H., Wang, Y., Sun, J., 2015b. Aerosol optical properties under the condition of heavy haze over an urban site of Beijing, China. Environ. Sci. Pollut. Res. 22, 1043–1053.

Chen, S.J., Liao, S.H., Jian, W.J., Lin, C.C., 1997. Particle size distribution of aerosol carbons in ambient air. Environ. Int. 23, 475–488.

Cheng, Y.F., Eichler, H., Wiedensohler, A., Heintzenberg, J., Zhang, Y.H., Hu, M., 2006. Mixing state of elemental carbon and non-light-absorbing aerosol components derived from in situ particle optical properties at Xinken in Pearl River Delta of China. J. Geophys. Res. 111, 4763–4773.

Cheng, Y.F., Wiedensohler, A., Eichler, H., Su, H., Gnauk, T., Brüggemann, E., 2008. Aerosol optical properties and related chemical apportionment at Xinken in Pearl River Delta of China. Atmos. Environ. 42, 6351–6372.

Cheung, H.C., Wang, T., Baumann, K., Guo, H., 2005. Influence of regional pollution outflow on the concentrations of fine particulate matter and visibility in the coastal area of southern China. Atmos. Environ. 39, 6463–6474.

Chow, J.C., Watson, J.G., Chen, L.W.A., Arnott, W.P., Moosmüller, H., Fung, K., 2004. Equivalence of elemental carbon by thermal/optical reflectance and transmittance with different temperature protocols. Environ. Sci. Technol. 38, 4414–4422.

Chow, J.C., Watson, J.G., Chen, L.W.A., Chang, M.C., Robinson, N.F., Trimble, D., 2007. The IMPROVE_A temperature protocol for thermal/optical carbon analysis: maintaining consistency with a long-term database. J. Air Waste Manage. Assoc. 57, 1014–1023.

Cozic, J., Verheggen, B., Weingartner, E., Crosier, J., Bower, K., Flynn, M., 2008. Chemical composition of free tropospheric aerosol for PM_1 and coarse mode at the high alpine site Jungfraujoch. Atmos. Chem. Phys. 8, 407–423.

Cusack, M., Pérez, N., Pey, J., Alastuey, A., Querol, X., 2013. Source apportionment of fine PM and sub-micron particle number concentrations at a regional background site in the western Mediterranean: a 2.5 year study. Atmos. Chem. Phys. 13, 5173–5187.

Deng, X., Tie, X., Wu, D., Zhou, X., Bi, X., Tan, H., 2008. Long-term trend of visibility and its characterizations in the Pearl River Delta (PRD) region, China. Atmos. Environ. 42, 1424–1435.

Feng, Y., Chen, Y., Guo, H., Zhi, G., Xiong, S., Li, J., 2009. Characteristics of organic and elemental carbon in $PM_{2.5}$ samples in Shanghai, China. Atmos. Res. 92, 434–442.

Fountoukis, C., Nenes, A., 2007. ISORROPIA II: a computationally efficient thermodynamic equilibrium model for K^+-Ca^{2+}-Mg^{2+}-NH_4^+-Na^+-SO_4^{2-}-NO_3^--Cl^--H_2O aerosols. Atmos. Chem. Phys. 7, 4639–4659.

Hand, J.L., Malm, W.C., 2007. Review of the IMPROVE Equation for Estimating Ambient Light Extinction Coefficients. CIRA, Colorado State University.

Hu, M., Wu, Z., Slanina, J., Lin, P., Liu, S., Zeng, L., 2008. Acidic gases, ammonia and water-soluble ions in $PM_{2.5}$ at a coastal site in the Pearl River Delta, China. Atmos. Environ. 42, 6310–6320.

Huang, R.J., Zhang, Y., Bozzetti, C., Ho, K.F., Cao, J.J., Han, Y., 2014. High secondary aerosol contribution to particulate pollution during haze events in China. Nature 514, 218–222.

Jung, J., Lee, H., Kim, Y.J., Liu, X., Zhang, Y., Gu, J., 2009. Aerosol chemistry and the effect of aerosol water content on visibility impairment and radiative forcing in Guangzhou during the 2006 Pearl River Delta campaign. J. Environ. Manag. 90, 3231–3244.

Lin, Z.J., Tao, J., Chai, F.H., Fan, S.J., Yue, J.H., Zhu, L.H., 2013. Impact of relative humidity and particles number size distribution on aerosol light extinction in the urban area of Guangzhou. Atmos. Chem. Phys. 13, 1115–1128.

Liu, X., Zhang, W., Wang, Z., Zhao, W., Tao, L., Yang, X., 2009a. Chemical composition and size distribution of secondary organic aerosol formed from the photooxidation of isoprene. J. Environ. Sci. 21, 1525–1531.

Liu, X., Zhang, Y., Jung, J., Gu, J., Li, Y., Guo, S., 2009b. Research on the hygroscopic properties of aerosols by measurement and modeling during CAREBeijing-2006. J. Geophys. Res. 114, 4723–4734.

Malm, W.C., Day, D.E., Kreidenweis, S.M., Collett, J.L., Lee, T., 2003. Humidity-dependent optical properties of fine particles during the big bend regional aerosol and visibility observational study. J. Geophys. Res. 108, 469–474.

Pitchford, M., Malm, W., Schichtel, B., Kumar, N., Lowenthal, D., Hand, J., 2007. Revised algorithm for estimating light extinction from IMPROVE particle speciation data. J. Air Waste Manage. Assoc. 57, 1326–1336.

Ramanathan, V., Feng, Y., 2009. Air pollution, greenhouse gases and climate change: global and regional perspectives. Atmos. Environ. 43, 37–50.

Samet, J.M., Dominici, F., Curriero, F.C., Coursac, I., Zeger, S.L., 2000. Fine particulate air pollution and mortality in 20 US cities, 1987–1994. N. Engl. J. Med. 343, 1742–1749.

Stelson, A., Seinfeld, J.H., 1982. Relative humidity and temperature dependence of the ammonium nitrate dissociation constant. Atmos. Environ. 16, 983–992.

Sun, Y.L., Zhang, Q., Schwab, J.J., Chen, W.N., Bae, M.S., Lin, Y.C., 2011. A case study of aerosol processing and evolution in summer in New York City. Atmos. Chem. Phys. Discuss. 11, 25751–25784.

Tao, J., Zhang, L., Ho, K., Zhang, R., Lin, Z., Zhang, Z., 2014. Impact of PM$_{2.5}$ chemical compositions on aerosol light scattering in Guangzhou - the largest megacity in South China. Atmos. Res. 135–136, 48–58.

Tao, J., Zhang, L., Gao, J., Wang, H., Chai, F., Wang, S., 2015. Aerosol chemical composition and light scattering during a winter season in Beijing. Atmos. Environ. 110, 36–44.

Tao, J., Zhang, L., Cao, J., Zhong, L., Chen, D., Yang, Y., 2017. Source apportionment of PM$_{2.5}$ at urban and suburban areas of the Pearl River Delta region, south China—with emphasis on ship emissions. Sci. Total Environ. 574, 1559–1570.

Wang, T., Poon, C.N., Kwok, Y.H., 2003. Characterizing the temporal variability and emission patterns of pollution plumes in the Pearl River Delta of China. Atmos. Environ. 37, 3539–3550.

Wang, Y.Q., Zhang, X.Y., Draxler, R.R., 2009. TrajStat: GIS-based software that uses various trajectory statistical analysis methods to identify potential sources from long-term air pollution measurement data. Environ. Model. Softw. 24, 938–939.

Watson, J.G., 2002. Visibility: science and regulation. J. Air Waste Manage. Assoc. 52, 628–713.

Weingartner, E., Saathoff, H., Schnaiter, M., Streit, N., Bitnar, B., Baltensperger, U., 2003. Absorption of light by soot particles: determination of the absorption coefficient by means of aethalometers. J. Aerosol Sci. 34, 1445–1463.

Wu, D., Mao, J., Deng, X., Tie, X., Zhang, Y., Zeng, L., 2009. Black carbon aerosols and their radiative properties in the Pearl River Delta region. Sci. China Earth Sci. 52, 1152–1163.

Wu, Y., Zhang, R., Pu, Y., Zhang, L., Ho, K., Fu, C.B., 2012. Aerosol optical properties observed at a semi-arid rural site in northeastern China. Aerosol Air Qual. Res. 12, 503–514.

Wu, D., Wu, C., Liao, B., Chen, H., Wu, M., Li, F., 2013. Black carbon over the South China Sea and in various continental locations in South China. Atmos. Chem. Phys. 13, 12257–12270.

Yan, P., Tang, J., Huang, J., Mao, J., Zhou, X., Liu, Q., 2008. The measurement of aerosol optical properties at a rural site in Northern China. Atmos. Chem. Phys. 8, 2229–2242.

Yue, D.L., Hu, M., Wu, Z.J., Guo, S., Wen, M.T., Nowak, A., 2010. Variation of particle number size distributions and chemical compositions at the urban and downwind regional sites in the Pearl River Delta during summertime pollution episodes. Atmos. Chem. Phys. 10, 9431–9439.

Zhang, Z., Engling, G., Lin, C.Y., Chou, C.K., Lung, S.C.C., Chang, S.Y., 2010. Chemical speciation, transport and contribution of biomass burning smoke to ambient aerosol in Guangzhou, a mega city of China. Atmos. Environ. 44, 3187–3195.

Zhang, R., Jing, J., Tao, J., Hsu, S.C., Wang, G., Cao, J., 2013. Chemical characterization and source apportionment of PM$_{2.5}$ in Beijing: seasonal perspective. Atmos. Chem. Phys. 13, 7053–7074.